Modeling and evaluating the performance of Brillouin distributed optical fiber sensors

Marcelo A. Soto[*] and Luc Thévenaz

EPFL Swiss Federal Institute of Technology, Institute of Electrical Engineering, SCI STI LT, Station 11, CH-1015 Lausanne, Switzerland
[*]marcelo.soto@epfl.ch

Abstract: A thorough analysis of the key factors impacting on the performance of Brillouin distributed optical fiber sensors is presented. An analytical expression is derived to estimate the error on the determination of the Brillouin peak gain frequency, based for the first time on real experimental conditions. This expression is experimentally validated, and describes how this frequency uncertainty depends on measurement parameters, such as Brillouin gain linewidth, frequency scanning step and signal-to-noise ratio. Based on the model leading to this expression and considering the limitations imposed by nonlinear effects and pump depletion, a figure-of-merit is proposed to fairly compare the performance of Brillouin distributed sensing systems. This figure-of-merit offers to the research community and to potential users the possibility to evaluate with an objective metric the real performance gain resulting from any proposed configuration.

OCIS codes: (060.2310) Fiber optics; (060.2370) Fiber optics sensors; (290.5900) Scattering, stimulated Brillouin; (060.4370) Nonlinear optics, fibers.

References and links

1. T. Horiguchi, K. Shimizu, T. Kurashima, M. Tateda, and Y. Koyamada, "Development of a distributed sensing technique using Brillouin scattering," J. Lightwave Technol. **13**(7), 1296–1302 (1995).
2. K. Hotate, "Measurement of Brillouin gain spectrum distribution along an optical fiber using a correlation-based technique-proposal, experiment and simulation," IEICE Trans. Electron. **E83-C**(3), 405–411 (2000).
3. X. Bao, A. Brown, M. Demerchant, and J. Smith, "Characterization of the Brillouin-loss spectrum of single-mode fibers by use of very short (<10-ns) pulses," Opt. Lett. **24**(8), 510–512 (1999).
4. K. Kishida and C.-H. Li, "Pulse pre-pump-BOTDA technology for new generation of distributed strain measuring system," in *Proc. Structural Health Monitoring and Intelligent Infrastructure* (Taylor and Francis, 2006), pp. 471–477.
5. A. W. Brown, B. G. Colpitts, and K. Brown, "Dark-pulse Brillouin optical time-domain sensor with 20-mm spatial resolution," J. Lightwave Technol. **25**(1), 381–386 (2007).
6. W. Li, X. Bao, Y. Li, and L. Chen, "Differential pulse-width pair BOTDA for high spatial resolution sensing," Opt. Express **16**(26), 21616–21625 (2008).
7. Y. Dong, X. Bao, and W. Li, "Differential Brillouin gain for improving the temperature accuracy and spatial resolution in a long-distance distributed fiber sensor," Appl. Opt. **48**(22), 4297–4301 (2009).
8. Y. Dong, H. Zhang, L. Chen, and X. Bao, "2 cm spatial-resolution and 2 km range Brillouin optical fiber sensor using a transient differential pulse pair," Appl. Opt. **51**(9), 1229–1235 (2012).
9. S. M. Foaleng, M. Tur, J.-C. Beugnot, and L. Thévenaz, "High spatial and spectral resolution long-range sensing using Brillouin echoes," J. Lightwave Technol. **28**(20), 2993–3003 (2010).
10. K. Y. Song, S. Chin, N. Primerov, and L. Thévenaz, "Time-domain distributed fiber sensor with 1 cm spatial resolution based on Brillouin dynamic grating," J. Lightwave Technol. **28**(14), 2062–2067 (2010).
11. Y. Dong, L. Chen, and X. Bao, "Time-division multiplexing-based BOTDA over 100 km sensing length," Opt. Lett. **36**(2), 277–279 (2011).
12. Y. Dong, L. Chen, and X. Bao, "Extending the sensing range of Brillouin optical time-domain analysis combining frequency-division multiplexing and in-line EDFAs," J. Lightwave Tech. **30**(8), 1161–1167 (2012).
13. M. N. Alahbabi, Y. T. Cho, and T. P. Newson, "150-km-range distributed temperature sensor based on coherent detection of spontaneous Brillouin backscatter and in-line Raman amplification," J. Opt. Soc. Am. B **22**(6), 1321–1324 (2005).
14. F. Rodriguez-Barrios, S. Martin-Lopez, A. Carrasco-Sanz, P. Corredera, J. D. Ania-Castanon, L. Thévenaz, and M. Gonzalez-Herraez, "Distributed Brillouin fiber sensor assisted by first-order Raman amplification," J. Lightwave Technol. **28**(15), 2162–2172 (2010).

15. S. Martin-Lopez, M. Alcon-Camas, F. Rodriguez, P. Corredera, J. D. Ania-Castañon, L. Thévenaz, and M. Gonzalez-Herraez, "Brillouin optical time-domain analysis assisted by second-order Raman amplification," Opt. Express **18**(18), 18769–18778 (2010).
16. M. A. Soto, G. Bolognini, and F. Di Pasquale, "Optimization of long-range BOTDA sensors with high resolution using first-order bi-directional Raman amplification," Opt. Express **19**(5), 4444–4457 (2011).
17. X. Angulo-Vinuesa, S. Martin-Lopez, J. Nuño, P. Corredera, J. D. Ania-Castañon, L. Thévenaz, and M. González-Herráez, "Raman-assisted Brillouin distributed temperature sensor over 100 km featuring 2 meter resolution and 1.2°C uncertainty," J. Lightwave Technol. **30**(8), 1060–1065 (2012).
18. X. Angulo-Vinuesa, S. Martin-Lopez, P. Corredera, and M. González-Herraez, "Raman-assisted Brillouin optical time-domain analysis with sub-meter resolution over 100 km," Opt. Express **20**(11), 12147–12154 (2012).
19. M. A. Soto, G. Bolognini, F. Di Pasquale, and L. Thévenaz, "Simplex-coded BOTDA fiber sensor with 1 m spatial resolution over a 50 km range," Opt. Lett. **35**(2), 259–261 (2010).
20. H. Liang, W. Li, N. Linze, L. Chen, and X. Bao, "High-resolution DPP-BOTDA over 50 km LEAF using return-to-zero coded pulses," Opt. Lett. **35**(10), 1503–1505 (2010).
21. S. Le Floch, F. Sauser, M. A. Soto, and L. Thévenaz, "Time/frequency coding for Brillouin distributed sensors," Proc. SPIE **8421**, 84211J (2012).
22. M. A. Soto, S. Le Floch, and L. Thévenaz, "Bipolar optical pulse coding for performance enhancement in BOTDA sensors," Opt. Express **21**(14), 16390–16397 (2013).
23. M. A. Soto, G. Bolognini, and F. Di Pasquale, "Analysis of pulse modulation format in coded BOTDA sensors," Opt. Express **18**(14), 14878–14892 (2010).
24. M. A. Soto, G. Bolognini, and F. Di Pasquale, "Long-range simplex-coded BOTDA sensor over 120 km distance employing optical preamplification," Opt. Lett. **36**(2), 232–234 (2011).
25. M. A. Soto, M. Taki, G. Bolognini, and F. Di Pasquale, "Optimization of a DPP-BOTDA sensor with 25 cm spatial resolution over 60 km standard single-mode fiber using Simplex codes and optical pre-amplification," Opt. Express **20**(7), 6860–6869 (2012).
26. S. Le Floch, F. Sauser, M. Llera, M. A. Soto, and L. Thévenaz, "Colour simplex coding for Brillouin distributed sensors," Proc. SPIE **8794**, 879437 (2013).
27. X.-H. Jia, Y.-J. Rao, K. Deng, Z.-X. Yang, L. Chang, C. Zhang, and Z.-L. Ran, "Experimental demonstration on 2.5-m spatial resolution and 1°C temperature uncertainty over long-distance BOTDA with combined Raman amplification and optical pulse coding," IEEE Photonics Technol. Lett. **23**(7), 435–437 (2011).
28. M. Taki, M. A. Soto, G. Bolognini, and F. Di Pasquale, "Study of Raman amplification in DPP-BOTDA sensing employing Simplex coding for sub-meter scale spatial resolution over long fiber distances," Meas. Sci. Technol. **24**(9), 094018 (2013).
29. M. A. Soto, G. Bolognini, and F. Di Pasquale, "Simplex-coded BOTDA sensor over 120 km SMF with 1 m spatial resolution assisted by optimized bidirectional Raman amplification," IEEE Photonics Technol. Lett. **24**(20), 1823–1826 (2012).
30. M. A. Soto, X. Angulo-Vinuesa, S. Martin-Lopez, S.-H. Chin, J. D. Ania-Castañon, P. Corredera, E. Rochat, M. Gonzalez-Herraez, and L. Thevenaz, "Extending the real remoteness of long-range Brillouin optical time-domain fiber analyzers," J. Lightwave Technol. **32**(1), 152–162 (2014).
31. P. H. Richter, "Estimating errors in least-squares fitting," Telecommun. Data Acquisition Prog. Rep. **42**(122), 107–137 (1995).
32. L. Thévenaz, S. F. Mafang, and J. Lin, "Effect of pulse depletion in a Brillouin optical time-domain analysis system," Opt. Express **21**(12), 14017–14035 (2013).
33. S. M. Foaleng and L. Thévenaz, "Impact of Raman scattering and modulation instability on the performances of Brillouin sensors," Proc. SPIE **7753**, 77539V (2011).
34. S. Diaz, S. Foaleng Mafang, M. Lopez-Amo, and L. Thevenaz, "A high-performance optical time-domain Brillouin distributed fiber sensor," IEEE Sens. J. **8**(7), 1268–1272 (2008).
35. L. Thévenaz, S. Le Floch, D. Alasia, and J. Troger, "Novel schemes for optical signal generation using laser injection locking with application to Brillouin sensing," Meas. Sci. Technol. **15**(8), 1519–1524 (2004).
36. J.-C. Beugnot, M. Tur, S. F. Mafang, and L. Thévenaz, "Distributed Brillouin sensing with sub-meter spatial resolution: modeling and processing," Opt. Express **19**(8), 7381–7397 (2011).
37. X. Bao, D. J. Webb, and D. A. Jackson, "22-km distributed temperature sensor using Brillouin gain in an optical fiber," Opt. Lett. **18**(7), 552–554 (1993).
38. X. Bao, D. J. Webb, and D. A. Jackson, "32-km distributed temperature sensor based on Brillouin loss in an optical fiber," Opt. Lett. **18**(18), 1561–1563 (1993).
39. X. Bao, J. Dhliwayo, N. Heron, D. J. Webb, and D. A. Jackson, "Experimental and theoretical studies on a distributed temperature sensor based on Brillouin scattering," J. Lightwave Technol. **13**(7), 1340–1348 (1995).
40. L. Thevenaz, M. Nikles, A. Fellay, M. Facchini, and P. A. Robert, "Applications of distributed Brillouin fiber sensing," in *International Conference on Applied Optical Metrology* (SPIE, 1998), pp. 374–381.
41. V. Lecœuche, D. J. Webb, C. N. Pannell, and D. A. Jackson, "25 km Brillouin based single-ended distributed fibre sensor for threshold detection of temperature or strain," Opt. Commun. **168**(1-4), 95–102 (1999).
42. Y. Dong, L. Chen, and X. Bao, "System optimization of a long-range Brillouin-loss-based distributed fiber sensor," Appl. Opt. **49**(27), 5020–5025 (2010).
43. X.-H. Jia, Y.-J. Rao, Z.-N. Wang, W.-L. Zhang, Y. Jiang, J.-M. Zhu, and Z.-X. Yang, "Towards fully distributed amplification and high-performance long-range distributed sensing based on random fiber laser," Proc. SPIE **8421**, 842127 (2012).

44. Z. Yang, X. Hong, J. Wu, H. Guo, and J. Lin, "Theoretical and experimental investigation of an 82-km-long distributed Brillouin fiber sensor based on double sideband modulated probe wave," Opt. Eng. **51**(12), 124402 (2012).
45. J. Hu, X. Zhang, Y. Yao, and X. Zhao, "A BOTDA with break interrogation function over 72 km sensing length," Opt. Express **21**(1), 145–153 (2013).
46. X.-H. Jia, Y.-J. Rao, Z.-N. Wang, W.-L. Zhang, C.-X. Yuan, X.-D. Yan, J. Li, H. Wu, Y.-Y. Zhu, and F. Peng, "Distributed Raman amplification using ultra-long fiber laser with a ring cavity: characteristics and sensing application," Opt. Express **21**(18), 21208–21217 (2013).
47. X.-H. Jia, Y.-J. Rao, C.-X. Yuan, J. Li, X.-D. Yan, Z.-N. Wang, W.-L. Zhang, H. Wu, Y.-Y. Zhu, and F. Peng, "Hybrid distributed Raman amplification combining random fiber laser based 2nd-order and low-noise LD based 1st-order pumping," Opt. Express **21**(21), 24611–24619 (2013).

1. Introduction

During the past few years Brillouin-based distributed optical fiber sensing has been turning into one of the most vivid fields of research in optical fiber sensing, mainly due to its ability to provide distributed temperature and strain measurements along several tens of km of optical fiber with spatial resolution values down to the centimeter scale [1]. Actually, thanks to advanced and ingenious techniques, remarkable progresses have been recently reported. On the one hand, the spatial resolution has been improved by at least 2 orders of magnitude from meter to centimeter scale using methods based on correlation-domain, differential pulses, and dynamic gratings, among others [2–10]. On the other hand, the distance range has been extended from some 30 km up to 150 km by using time-division multiplexing [11], frequency-division multiplexing [12], remote optical amplification [13–18], smart pump pulse coding techniques [19–26], or combination of these last two methods [27–30].

However, it still remains uneasy for an external observer to fairly evaluate the real progresses reported in the abundance of recent publications. There is currently no objective metric based on a rationale to evaluate the impact of a proposed technique in term of performance gain. For instance, how is it possible to compare a sensor achieving a 2 m spatial resolution with a 2 MHz Brillouin shift frequency accuracy over 100 km [11], to a sensor showing a 3 m spatial resolution with 3 MHz frequency accuracy over 120 km [24]? Do they provide a better performance than realizing a 5 cm spatial resolution over 5 km with 0.5 MHz frequency accuracy [9]?

No simple way to assess these different results is identified today and the only quantity sometimes used for comparison is the equivalent number of resolved sensing points, i.e. the ratio between the maximum sensing range and the spatial resolution. However this quantity does not take into account other important parameters such as the measurand resolution or the number of acquired/averaged traces, which is directly related to the measurement time. It also assumes that extending the sensing range and sharpening the spatial resolution have a proportional impact, which turns out to be much too simplistic as proved hereafter.

The purpose of this paper is to study the impact of the different variables in the measuring process on the sensor response and the final measurement uncertainty. The analysis also includes the fitting procedure required to estimate the Brillouin peak gain frequency (the so-called Brillouin frequency shift (BFS) [1]), which ultimately contains the distributed temperature and strain information. More specifically, the impact of the measurement parameters on the error of the BFS estimated from a quadratic least-square fitting process [31] is analyzed, so that a novel expression for the error on the BFS in Brillouin-based distributed sensors is derived and justified by its experimental validation. Then, a figure-of-merit (FoM) can be formulated combining this expression with a simple and universal model based on a generic distributed Brillouin sensor. This FoM is simply defined to be proportional to the signal-to-noise ratio (SNR) of the measurement, with some simple added considerations based on the limitations brought by pump depletion [32] and by other nonlinear effects, such as modulation instability and forward Raman scattering [33]. Therefore, any real progress offered by novel techniques should have the effect to normally make this FoM larger, so that the real performance improvement can be rigorously quantified.

2. Response of BOTDA sensors

In Brillouin optical-time domain analysis (BOTDA) based sensors a pulsed pump signal interacts with a continuous wave (CW) probe signal through stimulated Brillouin scattering (SBS) [1]. A simple scheme showing the implementation of a generic BOTDA sensor is depicted in Fig. 1. The light from a narrowband laser is split into two arms to generate both the pulsed pump and the CW probe signals. The upper branch in the figure shows the generation of the pump signal, in which the CW laser light is intensity modulated by a pulse shaping device that can be an electro-optic modulator, a semiconductor optical amplifier or any other type of modulating device with high extinction ratio. The peak power of the pulses may be boosted by an optical amplifier to launch high-peak power pulses into the fiber. On the other hand, the lower branch in Fig. 1 shows the generation of the probe signal through an optical frequency shifting device, in which the frequency shift can be precisely controlled. A common implementation is realized using an electro-optic modulator driven by a microwave signal in order to generate a double-sideband suppressed carrier CW probe wave, in which case one of the sidebands must be filtered out before detection [34]. A polarization scrambler or polarization switch (placed in the pump and/or probe arm) is typically employed to get rid of the spatial oscillations caused by the polarization-dependent Brillouin gain.
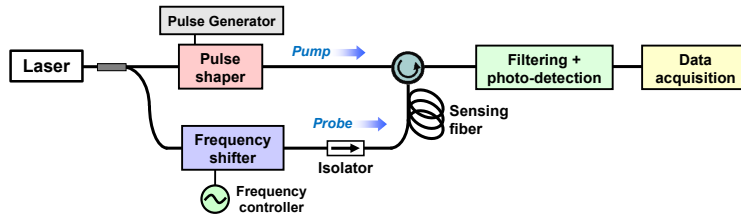

Fig. 1. Generic BOTDA sensor scheme.

While the frequency difference between pump and probe signals is scanned around the Brillouin frequency of the sensing fiber (through the frequency control, which is normally a microwave signal that modulates the CW probe), a data acquisition system is used to record the BOTDA time-traces at different frequency offsets. Usually a fiber Bragg grating (BFG) or other narrowband optical filter is used before the photo-detection to filter out unwanted spectral components, such as the Rayleigh backscattered light from the pump. It must be mentioned that the development presented in this paper is not restricted to a particular configuration and it applies to any BOTDA system implementing the interaction between a coherent pulsed signal with a frequency-shifted continuous coherent lightwave, for instance employing 2 frequency-locked lasers [3,35]. All elements that are not strictly essential for the basic operation of the BOTDA sensor are not represented in Fig. 1, since they can be considered like sophistications and are countlessly diversified.

If a Brillouin gain configuration is assumed for simplicity (i.e. the pump frequency is higher than the frequency of the CW probe component that is detected at the receiver), and without bringing restrictions to the analysis as justified later, the measured CW probe signal is amplified by stimulated Brillouin scattering while the pulsed pump propagates along the fiber, as shown in Fig. 2.
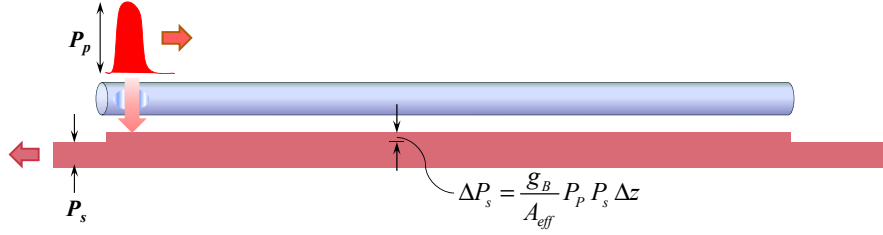
$$\Delta P_s = \frac{g_B}{A_{eff}} P_P P_s \Delta z$$

Fig. 2. Interacting signals in a generic BOTDA sensor. A light pulse of power P_P – called pump – interacts with a continuous wave of power P_S – called probe or signal – through the intercession of an idler acoustic wave if a strict phase matching condition is satisfied. Phase matching depends on the frequency difference between pump and probe and gives rise to a local power transfer ΔP_s between the interacting optical waves.

For a fixed frequency difference between the interacting optical signals, the amount of power transferred from the pump $P_p(z)$ to the probe $P_s(z)$ is given by:

$$\Delta P_s(z) = P_s(z)\left[\exp\left(\frac{g_B(z)}{A_{eff}} P_P(z)\Delta z \right) - 1 \right], \tag{1}$$

where $g_B(z)$ represents the local Brillouin gain coefficient, A_{eff} is the nonlinear effective area of the guided mode and Δz is the interaction length, which is equivalent to the spatial resolution and determined by the pump pulse half duration multiplied by the group velocity of the guided mode. The quantity given by Eq. (1) actually corresponds to the *local sensor response*, in which the gain value $g_B(z)$ is considered for the given frequency difference and is assumed to be constant over the interaction length Δz. This response is, in principle, valid for pulses longer than the acoustic amplitude lifetime $\tau = 11$ ns, so that the stationary approximation for the acoustic wave can be used. However, it must be pointed out that advanced configurations using shorter pulses for high spatial resolution, based on the pre-excitation of the acoustic wave, turn out to experience a power transfer that is also given by Eq. (1), provided that the pre-excitation is long enough to let the acoustic wave reach its steady state value [25,36], so that this expression can safely be employed for all ranges of spatial resolution.

In order to avoid pump depletion (in Brillouin gain configuration) or excess amplification (in Brillouin loss configuration), BOTDA sensors operate in a small gain regime [32], i.e. $\Delta P_s(z) / P_s(z) << 0.1$; and therefore, the local sensor response defined by Eq. (1) can be safely simplified as:

$$\Delta P_s(z) = \frac{g_B(z)}{A_{eff}} P_P(z) P_s(z) \Delta z. \tag{2}$$

In most high performance sensors this relative power transfer is actually in the 1% range or below. Actually, the absolute value of the sensor response turns out to be similar in gain and loss configurations under small amplification.

Under the undepleted pump approximation it is possible to assume that the accumulated power that is transferred from the pump to the probe along the fiber is negligible, which is a necessary experimental condition to avoid systematic errors on the determination of the Brillouin frequency shift [32]. Negligible depletion actually makes the pump power simply decay exponentially during propagation as a result of the linear fiber loss α_p at the pump wavelength. Similarly, the small gain approximation makes the probe power P_s negligibly modified by the interaction and therefore predominantly ruled by the linear loss α_s at the probe wavelength. Losses experienced by pump and probe are identical in normal conditions due to their very close spectral vicinity; however, for the sake of generality some of the following expressions describe the interaction using two distinct loss coefficients. This distinction is mostly irrelevant from a practical point of view, but will be later helpful for the

physical interpretation. Under these realistic assumptions the local sensor response $\Delta P_s(z)$ can be calculated as a perturbation and simplifies to a z-independent quantity for identical losses and for uniform Brillouin linear gain g_B:

$$\Delta P_s(z) = \frac{g_B(z)}{A_{eff}} P_{Pi} \exp\left(-\alpha_p z\right) P_{si} \exp\left[-\alpha_s(L-z)\right]\Delta z$$

$$= \frac{g_B(z)}{A_{eff}} P_{Pi} P_{si} \exp\left(-\alpha L\right)\Delta z, \qquad \text{for } \alpha = \alpha_p = \alpha_s, \tag{3}$$

where P_{Pi} and P_{si} are the input pump and probe powers, respectively. This situation directly results from the counter-propagative configuration required for the interacting optical waves in stimulated Brillouin scattering, as shown in Fig. 3: the power transfer is scaled by the product of pump and probe powers that is constant at any position z. In other words, while the pump is large at position $z = 0$, the probe is weak since it has been fully attenuated by linear loss along the full fiber length L. The power situation of the two waves is exactly reversed in the same proportion at $z = L$, and it can be even generalized that these powers are in exact inverse proportion at any position z for equal pump and probe linear losses, as described by Eq. (3).
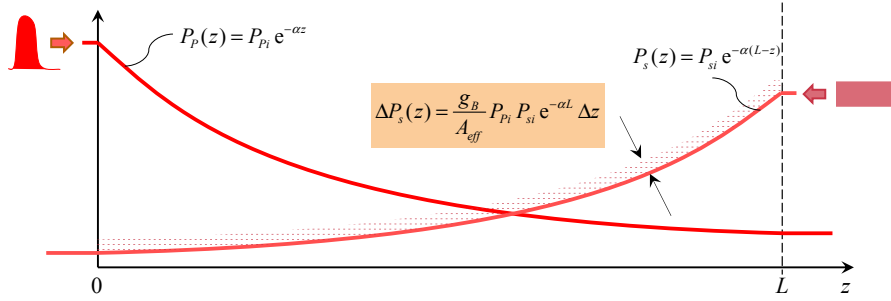

Fig. 3. The counter-propagative interacting signals in a BOTDA sensor experience linear loss and exponentially decay during their propagation. Since at each position z the Brillouin response is proportional to the product of the pump pulse of power $P_P(z)$ by the CW probe power $P_S(z)$ they show complementary amplitudes as a result of the counter-propagating situation and their product is invariant with position z.

As previously mentioned, the expression in Eq. (3) corresponds to the local sensor response, however, the power transferred at a position z is measured at the fiber near end (position $z = 0$) and, since the probe signal must be conveyed from z to 0, it experiences the effect of the linear fiber attenuation α_s over this distance. As a result, the sensor response ΔP_s measured at the fiber near end is given by the following expression:

$$\Delta P_s^0(z) = \Delta P_s(z)\exp\left(-\alpha_s z\right) = \frac{g_B(z)}{A_{eff}} P_{Pi} \exp\left(-\alpha_p z\right) P_{si} \exp\left(-\alpha_s L\right)\Delta z. \tag{4}$$

This expression actually corresponds to the *measured sensor response* and is proportional to the local gain coefficient $g_B(z)/A_{eff}$, the spatial resolution Δz, the local pump power $P_{Pi}\exp(-\alpha_p z)$ and the CW probe power $P_{si}\exp(-\alpha_s L)$ at the fiber near end in absence of SBS interaction. Thus, the local Brillouin gain associated to this response as a function of z can simply be obtained dividing Eq. (4) by the CW probe power measured at the receiver, yielding:

$$Gain(z) = \frac{\Delta P_s^0(z)}{P_{si}\exp(-\alpha_s L)} = \frac{g_B(z)}{A_{eff}} P_{Pi} \exp\left(-\alpha_p z\right)\Delta z. \tag{5}$$

Thus, the local gain observed at the fiber near end is proportional to the local Brillouin gain coefficient $g_B(z)$ (in the small gain approximation) and the local pump power. If the Brillouin gain is uniform along the fiber, the response traces will show an exponential decrease as a function of the distance z along the fiber; however, if the Brillouin gain is not uniform, then the position dependence of $g_B(z)$ will determine a gain profile different from the conventional exponential decay. This will be also the case if the pump is subject to distributed amplification or any type of nonlinear interaction.

Assuming that the interacting waves only experience the same linear loss during their propagation, it is evident from Eqs. (4) and (5) that the more distant the position z, the smaller the measured sensor response, and the worst case therefore corresponds to an interaction taking place close to the fiber far end at $z = L$. Consequently, under standard BOTDA conditions, the sensor accuracy must be essentially proved with measurements performed at the far end where the measured sensor response is:

$$\Delta P_s^0 \left(z = L \right) = \frac{g_B}{A_{eff}} P_{Pi} P_{si} \exp\left(-2\alpha L\right) \Delta z. \tag{6}$$

Note that, even though the local gain at position L shows an exponential attenuation as $\exp(-\alpha L)$ according to Eq. (5), the absolute power signal variation that is measured by the sensor from an interaction at the fiber far end ($z = L$) is scaled by a factor $\exp(-2\alpha L)$, as expressed by Eq. (6). This fact is essential to grasp how the sensing distance impacts on the signal-to-noise ratio (SNR) of BOTDA traces, in particular at the far end where the lowest absolute signal amplitude has to be detected. Actually, the effect of the fiber attenuation turns out to be doubled when compared to a one-way propagation; consequently, using standard values for the linear loss at 1550 nm it can be concluded that increasing the sensing range by 7.5 km raises a difficulty similar to decreasing the spatial resolution by a factor 2 (in both cases the measured sensor response at $z = L$ and the respective SNR are reduced by 3 dB). Note that the attenuation on the sensor response can be widely compensated by using amplification before detection, though with the penalty of the amplifier noise figure. This possibility of amplification can be eventually considered as a technical sophistication to improve the figure-of-merit introduced later in this paper and will not be further considered here.

In order to experimentally verify the behavior of the measured sensor response at the far fiber end described by Eq. (6), measurements have been carried out using different fiber lengths and a setup based on Fig. 1. Considering that the analyzed distinct fiber segments might have different Brillouin gain coefficient g_B and different effective areas A_{eff}, the pump power launched into the fiber has been adjusted in order to provide the same maximum gain to the BOTDA traces at $z = 0$. This makes a fair comparison possible between the different tested fibers, all of standard type and showing a similar linear loss. Thus, the gain expressed by Eq. (5) at the fiber near end ($z = 0$) has been set to 3% at the peak Brillouin gain for all the measurements reported here. The spatial resolution and the number of averaged traces have been identically set to 2 m and 1000, respectively, for all measured fiber segments. Figure 4 shows the sensor response ΔP_s^0 (in dB scale) resulting from the Brillouin gain measured at the far end of several distinct fibers, with lengths ranging from 2 km up to 50 km. These measured power variations have been normalized to their value measured at $z = 0$, which has been set identical in term of gain for all tested fibers. In addition to the sensor response, Fig. 4 also shows the respective linear fitting (black dashed line) of the acquired data, whose slope is equal to -2α according to Eq. (6). This fitting results in an attenuation coefficient $\alpha = 0.211$ dB/km, which is in good agreement with standard values in single-mode fibers at 1550 nm.
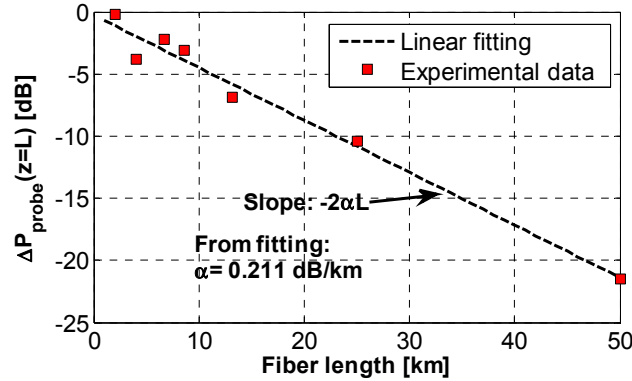
Fig. 4. Measured sensor response for an interaction taking place at the far end of sensing fibers with different length *L*. Data are normalized to the response obtained at the near end to better visualize the fiber length dependence.

3. Impact of the signal noise on the error of the estimated Brillouin frequency shift

In Brillouin distributed time-domain sensing the local Brillouin response is retrieved by measuring the probe signal power variations as a function of the distance for successive pump-probe frequency detuning. At each position the local spectral distribution of the Brillouin gain spectrum (BGS) can be reconstructed, as shown in Fig. 5, from which the local peak gain frequency is then estimated by a fitting procedure.
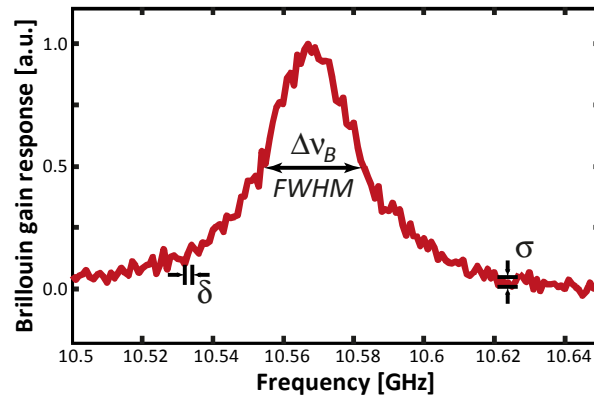

Fig. 5. Typical local Brillouin spectral response after normalization, measured by a distributed time-domain sensor. The distribution maps a resonant Lorentzian profile and the peak gain frequency must be determined to get an estimated value for the measurand. Noise on the signal (σ) induces uncertainty and the estimation of the peak gain frequency is subject to statistical errors, depending on the Brillouin FWHM ($\Delta\nu_B$) and the frequency step (δ) used to measure the gain spectrum.

A standard robust approach consists in making a rough estimate of the peak frequency and the peak gain value through a first pass, in order to discard all experimental points below a given fraction of the peak value (e.g. 50%). A numerical fit can then be performed over the kept points, which can be based on a limited number of degrees of freedom (e.g. parabolic fit) to optimize the robustness of the estimation.

Surprisingly, the estimation of the potential error on the Brillouin frequency shift for a given signal noise has been very poorly addressed in the literature so far. Only one relation has been proposed in a pioneering article on Brillouin fiber distributed sensing [1], claiming an unusual fourth root dependence on the SNR, without detailed justification and with no other dependence on the estimation procedure (i.e. on the type of curve fitting) or on

measurement conditions, such as the number of frequency points involved in the fitting (or equivalently the frequency sampling step).

In this work a new relation is established directly following the procedure used for fitting, by calculating the propagation of errors on the parameters obtained from a least-square parabolic fit [31], subject to given and equal stochastic errors σ on the measured gain spectral amplitudes (noise on the curve in Fig. 5). For this calculation a normalized gain response has been assumed, i.e. the response is 0 in absence of gain (far from the resonance) and is equal to 1 at the estimated peak response, as shown in Fig. 5. Under these assumptions, the noise amplitude σ is here defined as a fraction of this normalized response, directly representing the inverse of the local SNR on the trace at the peak gain frequency. If Δv_B is the estimated Brillouin full-width at half maximum (FWHM) of the resonance and δ is the frequency sampling step (i.e. the frequency increment between successive Brillouin intensity traces), the propagated error on the estimated resonance central frequency σ_v expresses as:

$$\sigma_v(z) = \sigma(z) \sqrt{\frac{3 \cdot \delta \cdot \Delta v_B}{8\sqrt{2}(1-\eta)^{3/2}}} = \frac{1}{SNR(z)} \sqrt{\frac{3 \cdot \delta \cdot \Delta v_B}{8\sqrt{2}(1-\eta)^{3/2}}}, \tag{7}$$

where η is the fraction of the peak level over which a quadratic least-square fitting is carried out, i.e. all frequency points above this level η are involved in the quadratic fitting (see Appendix for the details on the derivation of Eq. (7)). Thus, in the particular case of $\eta = 0.5$, i.e. when the quadratic fitting is performed taking in to account only the data points within the Brillouin FWHM Δv_B, Eq. (7) reduces to:

$$\sigma_v(z) = \sigma(z) \sqrt{\frac{3}{4} \delta \cdot \Delta v_B} = \frac{1}{SNR(z)} \sqrt{\frac{3}{4} \delta \cdot \Delta v_B}. \tag{8}$$

The validity of these expressions is subject to the condition $\delta \ll \Delta v_B$, which is equivalent to require a large number of frequency sampling points. Actually, as proved in the Appendix, the validity is already good for 3 or more frequency points. Another condition is that a prior rough estimate of the central frequency has been performed, so that the measured points considered for the estimation are evenly distributed around the expectation value of the peak gain frequency. These are no real limitations, since this is normally carried out in a standard measurement procedure. If the fraction η is different from 0.5, it just changes the multiplying constant on the right term of Eq. (7). Even though this relation is here established in the particular case of a parabolic fit, it is not expected to substantially differ for more elaborated fitting functions, except possibly in the numerical proportionality factor, but unlikely in the functional dependence of the parameters, as clarified in the Appendix.

It must be pointed out that logically this expression gives a strict proportionality between signal noise and frequency error, whereas the number of frequency sampling points has a direct scaling impact on the error of the estimation. Actually, Eqs. (7) and (8) are valid not only for BOTDA systems, but can also be applied to estimate the frequency error resulting from any Brillouin frequency shift estimation based on fitting a measured Brillouin spectrum, like Brillouin optical time-domain reflectometry (BOTDR) [13] or Brillouin optical correlation-domain systems [2]. It can be even generalized to any system in which the central value of a resonance must be evaluated by fitting experimental points obtained by a frequency scan.

In order to validate the expression proposed in Eq. (8), measurements along a 24.5 km-long standard single-mode fiber have been repeated varying the different parameters entering into this expression. First, the essential discrepancy with the formerly published relation in [1] has been checked, namely the inverse linear dependence on the SNR, fixing $\eta = 0.5$, the frequency step at 1 MHz and the FWHM at 58 MHz, which is obtained using a spatial resolution of 2 m.

Figure 6 shows the frequency error as a function of distance, calculated as the standard deviation of the experimental BFS obtained from the quadratic fitting process for the case of

10 (blue solid line) and 200 (red solid line) averaged traces. The standard deviation is calculated from a set of about 100 estimated BFS at close positions. The dashed lines in the figure represent the respective frequency error calculated using Eq. (8), based on the exponential dependency of the SNR measured in the traces. The exact inverse proportion between the frequency error and $SNR(z)$ is evident in the figure when considering the growth of the frequency error σ_v (z) $\sim 1/SNR(z)$ with distance, which nominally increases exponentially according to the one-way fiber attenuation coefficient (α = 0.22 dB/km, obtained in this case from fitting an exponential curve to the measured SNR as a function of the distance). In Fig. 6 the impact of trace averaging can also be observed, where the frequency error obtained at 24.5 km distance with 10 time-averaged traces is 3.21 MHz, which is improved down to 0.75 MHz with 200 averages. This corresponds to an improvement factor of 4.28 on the BFS accuracy, which is in good agreement with the improved SNR resulting from the additional averaging (note that increasing the trace averaging in a factor of 20 results in a $\sqrt{20} \approx 4.47$ better SNR).
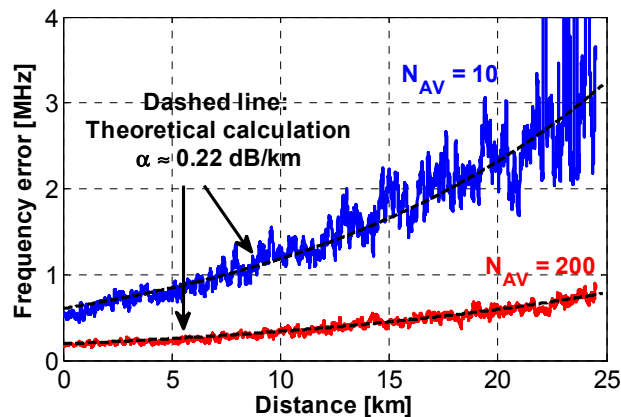

Fig. 6. Frequency error vs distance, measured as the standard deviation of the Brillouin frequency shift obtained for 10 and 200 time-averaged traces (blue and red solid lines). Dashed lines: theoretical calculation of the frequency error based on Eq. (8) and on the exponential behavior of the SNR measured in the time-traces at the maximum gain frequency (the attenuation factor α = 0.22 dB/km is obtained from fitting the measured SNR with an exponential curve).

According to Eq. (8), the number of averaged traces N_{AV} implicitly impacts on the frequency error by raising the SNR following a $1/\sqrt{N_{AV}}$ dependence, as illustrated in Fig. 7. This figure actually presents the frequency error at 24.5 km distance as a function of the number of averages when δ = 1 MHz, and Δv_B = 58 MHz (equivalent to 2 m spatial resolution). The dashed line in the figure corresponds to the theoretical frequency error estimated using Eq. (8), based on the SNR of the trace at the peak-gain frequency and at the far end of the fiber. It must be mentioned that this curve is not obtained by fitting, but is a prediction resulting from a single SNR measurement. Actually, in this case the SNR has been measured using 200 time-averaged traces and then estimated for other averaging numbers by applying the $1/\sqrt{N_{AV}}$ dependence.
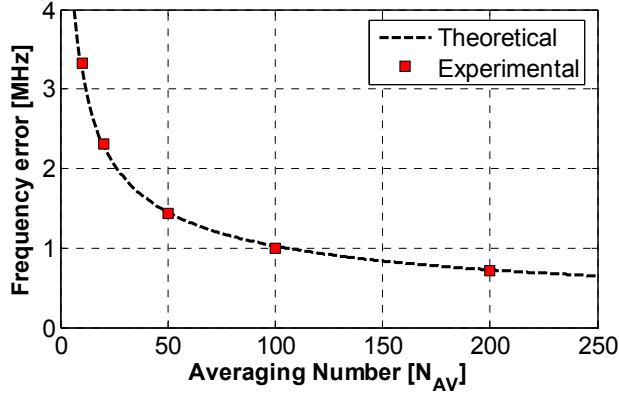
Fig. 7. Frequency error as a function of the number of time-averaged traces, at a 24.5 km distance. The theoretical curve (dashed line) is calculated using Eq. (8) (for $\delta = 1$ MHz, $\Delta v_B = 58$ MHz), based on the SNR calculated at the far fiber end of the time-trace at the peak gain frequency.

A remarkable agreement between the measured error values and the ones predicted by direct calculation employing Eq. (8) can be observed in Figs. 6 and 7. Actually, Fig. 8 compares the frequency error calculated theoretically using Eq. (8) and the error obtained from the standard deviation of the measured BFS (for 200 time-averaged traces). In this case $SNR(z)$ is evaluated at every fiber location (over the trace with the maximum gain) and then used to calculate the expected frequency error from Eq. (8) (using $\delta = 1$ MHz, and $\Delta v_B = 58$ MHz). It can be seen that all (blue) data points in Fig. 8, obtained by coupling the calculated and measured frequency errors at different positions along the fiber, are scattered along a straight line with unity slope, verifying the good agreement between predicted and experimental error values. The small frequency errors (around 0.2 MHz) in the figure represent the values obtained near the fiber input ($z = 0$) where the highest SNR is observed, while errors of about 0.8 MHz are obtained near the fiber far end ($z = 24.5$ km).
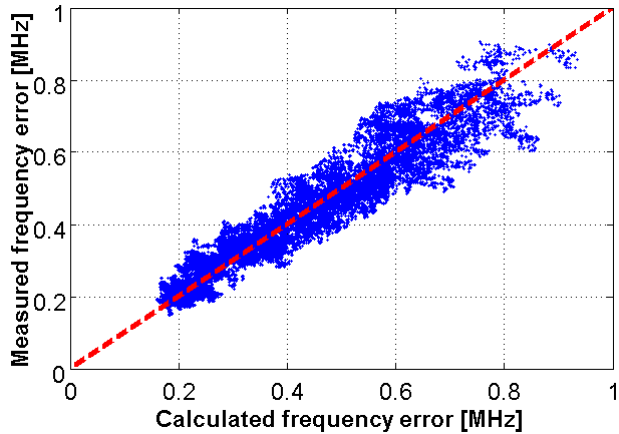

Fig. 8. Measured frequency error vs calculated frequency error (blue dots), when using 200 time-averaged traces. Red dashed line: Ideal case representing no difference between calculated and measured errors.

To evaluate the dependence of the measurand resolution on the frequency scan increment, σ_v has been evaluated at the far end of the fiber ($z = 24.5$ km). Figure 9 shows the measured and calculated frequency error as a function of the frequency increment when using 200 time-averaged traces and SNR = 9.4 dB (evaluated at the fiber far end from the temporal trace at the peak gain frequency). For a reliable comparison, the distributed BGS profile has been

measured by acquiring only one set of traces with a small frequency step (δ = 200 kHz); however, an undersampling has been voluntarily performed during the quadratic fitting process, so that the effective frequency step could be freely varied from 0.2 MHz up to 5 MHz using the same set of experimental time traces. This way, possible inaccuracies introduced by slowly varying noise and environmental conditions are suppressed, leading to a more reliable comparison. It can be observed that a small frequency step (i.e. when more data points are involved in the fitting of the gain spectrum) leads, as expected, to more accurate frequency measurements. Therefore, as shown in Fig. 9, if the frequency increment δ is larger, the frequency error grows with a factor proportional to $\sqrt{\delta}$, in full agreement with the model rooting Eq. (8).
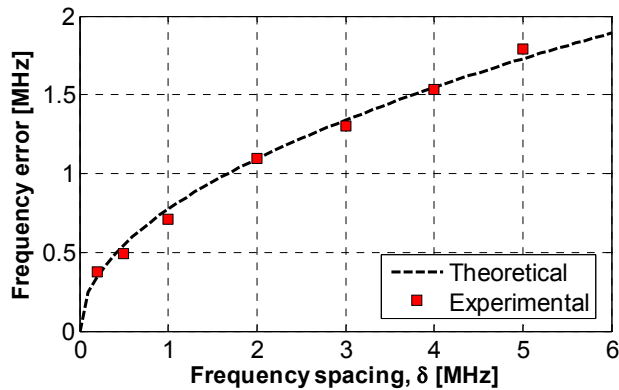

Fig. 9. Frequency error as a function of the frequency spacing, at 24.5 km distance and using 200 time-averaged traces. The theoretical curve (dashed line) is calculated using Eq. (8), for Δv_B = 58 MHz and SNR = 9.4 dB.

Finally, the impact of the Brillouin linewidth on the frequency error has been analyzed, as shown in Fig. 10. Here, the Brillouin linewidth has been simply changed using different pump pulse widths (between 10 ns and 60 ns). However, it is important to take into account that when the spatial resolution is varied, the local Brillouin gain changes, affecting the SNR of the traces accordingly. To evaluate the impact of the Brillouin spectral width only, the peak pump power has been adjusted in order to keep a constant Brillouin gain between measurements. This way, the SNR on the BOTDA traces at the peak frequency is the same for all measurements (SNR = 9.4 dB as in the previous case), making a reliable comparison possible between different Brillouin linewidth conditions.
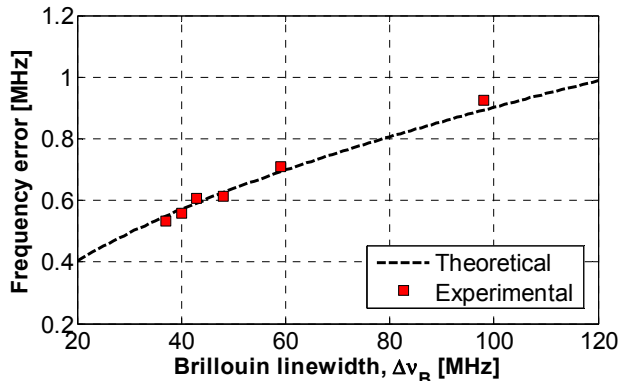

Fig. 10. Frequency error as a function of the FWHM Brillouin linewidth, at a 24.5 km distance and using 200 time-averaged traces. The theoretical curve (dashed line) is calculated using Eq. (8), for δ = 1 MHz and SNR = 9.4 dB.

Experimental results demonstrate with no ambiguity the relevance and the merits of Eq. (8) to estimate the frequency error of a Brillouin-based distributed optical fiber sensor. As previously mentioned, Eq. (8) assumes that the fitting is carried out considering all frequency

points within the Brillouin FWHM; however, as expressed in Eq. (7) the frequency error also depends on the discriminating level η from which the quadratic fitting is performed. In order to verify the accuracy of that more general expression, the BGS obtained from a single measurement has been repetitively fitted with different η levels. The frequency error estimated at 24.5 km distance (with δ = 1 MHz, Δv_B = 58 MHz, and SNR = 9.4 dB) is shown in Fig. 11, where it can be visually inspected how much the frequency error can be reduced if a broader spectral range (lower η level) is included in the fitting. This can be easily understood since the use of a lower η level increases the number of data fitting points and a more accurate evaluation of the peak frequency can thus be obtained. On the other hand, when the fitting is carried out including a smaller number of frequency points (higher η levels), the accuracy on the quadratic fitting is reduced, leading to higher error values.
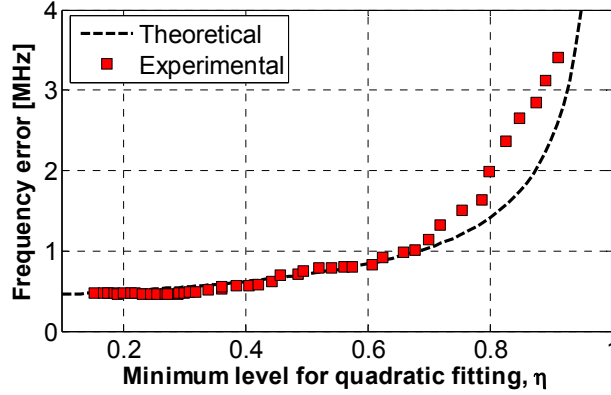

Fig. 11. Frequency error as a function of the threshold level used for the quadratic fitting, at a 24.5 km distance and using 200 time-averaged traces. The theoretical curve (dashed line) is calculated using Eq. (7), for δ = 1 MHz, Δv_B = 58 MHz and SNR = 9.4 dB.

The differences in Fig. 11 between the measured and calculated errors when η > 0.7 could be explained by the fact that a limited number of points is used for the quadratic fitting: actually, Eq. (7) (and hence Eq. (8)) has been obtained assuming that the number of frequency points involved in the fitting is much larger than 1 (see Appendix), a condition that is in general difficult to meet when η is close to 1. In addition, it is important to note that the first term in Eq. (24) might also impact on the frequency error at long distances if η is close to 1 since a reduced SNR makes it difficult to secure a perfect symmetry of the experimental spectrum subject to the fitting, i.e. a perfect centering on the expected peak gain frequency. Incidentally Fig. 11 shows that choosing η = 0.5 is a good compromise between accuracy and number of fitted points that ultimately decides the measurement time.

These experimental validations demonstrate that Eq. (7) is an expression based on a solid background to describe and predict the accuracy of a BOTDA sensor. Actually, by simply determining the SNR of the measured sensor response at any single fiber location z and at the peak gain frequency, the sensor performance can be fully predicted. For instance, the maximum reachable sensing distance can be easily estimated for a given accuracy, spatial resolution and averaging. Re-expressing Eq. (7) in the case of uniform linear loss α and Brillouin amplification g_B/A_{eff}, and assuming that the SNR of the sensor response is known at the fiber near end ($z = 0$) yields:

$$\sigma_v(z) = \frac{\exp(\alpha z)}{SNR(z=0)} \frac{\Delta z^0}{\Delta z} \sqrt{\frac{N_{AV}^0}{N_{AV}}} \sqrt{\frac{3 \cdot \delta \cdot \Delta v_B}{8\sqrt{2}(1-\eta)^{3/2}}}, \quad (9)$$

where Δz^0 and N_{AV}^0 are the spatial resolution and the number of averaging at which the SNR is evaluated, respectively. It is thus straightforward to determine the maximum distance z_{max} at which a given Brillouin frequency accuracy σ_v will be secured. This is exemplified in Fig. 12, which depicts the maximum sensing distance as a function of the target frequency uncertainty

and spatial resolution Δz, assuming that a realistic $SNR = 0$ dB is measured at the input fiber end with a spatial resolution $\Delta z^0 = 2$ m and no averaging (i.e. $N_{AV}^0 = 1$). It can be observed that a distance range $z_{max} = 50$ km can be reached while securing a frequency uncertainty of 2 MHz in standard conditions ($\alpha^{-1} = 22$ km, $\Delta \nu_B = 58$ MHz) with $N_{AV} = 1000$, $\delta = 1$ MHz, $\eta = 0.5$ and keeping the same spatial resolution of 2 m. However, if the frequency uncertainty is bound to a maximum of 1 MHz, the 50 km distance range can only be maintained by downgrading the spatial resolution to $\Delta z \approx 3.5$ m.
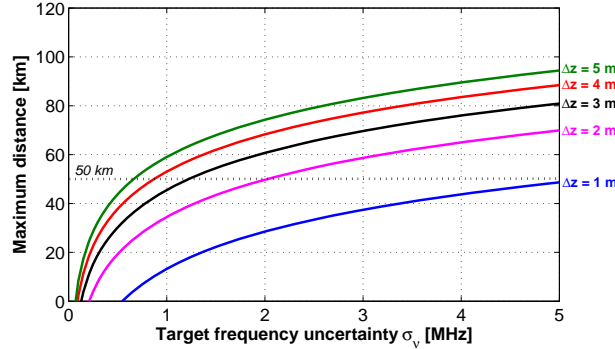

Fig. 12. Maximum sensing distance as a function of the frequency uncertainty and spatial resolution. The sensor response is predicted using Eq. (9) with $\alpha^{-1} = 22$ km, $N_{AV} = 1000$, $\delta = 1$ MHz, $\eta = 0.5$ and $\Delta z = 2$ m, under the realistic condition of a 0 dB SNR measured at the fiber near end ($z = 0$) with a spatial resolution $\Delta z^0 = 2$ m and $N_{AV}^0 = 1$.

Thus, as a clear outcome of this study, the SNR on the sensor response turns out to be the crucial parameter scaling the entire performance of the sensing system. In addition Eq. (9) is also an efficient tool to optimize the set of parameters chosen for the acquisition procedure. For instance, time averaging and frequency scanning step have a similar impact on the accuracy. Since setting a new frequency on a microwave generator takes in general a much longer time than individual time averaging, it may be more effective in some systems to make larger frequency steps while simultaneously increasing the number of time averages, to eventually improve the overall acquisition speed while securing the same measurement accuracy.

4. Figure-of-merit for distributed Brillouin optical fiber sensors

By analyzing the sensor response measured at the receiver as a function of the distance, as described in Eq. (6), the pump and probe input powers in this expression can be considered as fixed for all types of Brillouin-based sensors, since they are essentially limited by the critical power for other nonlinear effects [33] and depletion [32] in some cases. However, these two effects are actually scaled by the effective nonlinear length of the fiber $L_{eff} = (1 - \mathrm{e}^{-\alpha L})/\alpha$ that asymptotically tends towards α^{-1} for very long fibers. This means that distributed sensing systems employing short fibers ($L < \alpha^{-1}$) benefits from higher possible pump and probe signal powers, since they can be raised by a factor $1/(\alpha L_{eff})$ and this will eventually enhance the sensor response. This fact has to be considered for a fair comparison between high spatial resolution sensors (typically short distance) and long distance systems.

On the other hand, recent achievements for ultra-long sensing ranges have reported configurations in which an optical fiber twice longer than the actual sensing range is used [12,30]. In contrast to standard BOTDA configurations, in which both probe and pump experience the one-way fiber attenuation along the whole sensing fiber (as described in Fig. 3), in such a long-range fiber loop configuration, the probe signal experiences twice the sensing fiber attenuation (equivalent to the one-way attenuation along the whole fiber), while the active pump power is affected by the attenuation only along the sensing fiber [30]. This way, following the description presented in Section 2, the dependence of SNR at the receiver

on the sensing fiber length should be scaled by a factor $\exp(-3\alpha L)$ (where L corresponds to the sensing fiber length) and not by a factor $\exp(-2\alpha L)$ as in the standard fiber configuration, to take into account the probe propagation over the extra fiber length L. This issue should to be considered in the figure-of-merit since it has a significant impact on the SNR at the receiver, the probe signal being highly attenuated when long sensing ranges have to be covered. Thus, for instance, reaching a 100 km sensing distance using a 200 km fiber loop, in which the probe is attenuated by 40 dB, is much more challenging than using a 100 km fiber where the probe is attenuated by only 20 dB.

Another issue to include into the figure-of-merit is related to the number of time-averaged traces N_{AV} since, as reported in Fig. 7, the SNR can be arbitrarily increased in direct proportion to $\sqrt{N_{AV}}$ at the expense of a longer acquisition time. Although the number of averaged traces could be considered as a good indicator of the measurement time, some techniques are subject to an extra acquisition time since they require more than a single trace per frequency step; for instance, this is the case in methods employing differential measurements [6–9] or optical pulse coding [19–26], in which the measurement time depends on the number of averages N_{AV} and the number of different traces N_{Tr} required per frequency step. In order to consider the actual measurement time per scanned frequency, the total number of acquired traces $N_{Tr}N_{AV}$ has to be taken into account for a fair comparison. For instance, while the standard BOTDA scheme requires $N_{Tr} = 1$ [1], differential-pulse methods use $N_{Tr} = 2$ traces per scanned frequency [6–9]. On the other hand, in the case of using pulse coding [19–22], the number of coded traces N_{Tr} required at each frequency offset depends on the specific type of code being used in the sensor.

Based on the above-mentioned considerations and taking Eqs. (6)–(8) into account, the following unitless figure-of-merit (FoM) can be defined for distributed fiber sensors based on Brillouin optical time-domain analysis:

$$FoM = \frac{\left(\alpha L_{eff}\right)^2 \exp\left[(2+f_l)\alpha L\right]}{\Delta z \sqrt{N_{Tr}N_{AV}}} \frac{\sqrt{\delta \, \Delta\nu_B}}{\sigma_\nu},\qquad(10)$$

where consistent units have to be used and Δz is normalized to 1 m. Note that in Eq. (10), L is the sensing fiber length, and f_l is a parameter that takes into account the fiber configuration: $f_l = 0$ for the standard fiber configuration (i.e. when the total fiber length is equal to L) and $f_l = 1$ for the fiber loop configuration [12,30], in which half of the total fiber length is employed for sensing (i.e. when the total fiber length is equal to $2L$).

This FoM turns out to be equal to 1 for a typical commercial sensor of distance range $L = 30$ km, spatial resolution of $\Delta z = 1$ m and error on the Brillouin frequency of $\sigma_\nu = 1$ MHz, obtained with a standard BOTDA method (i.e. $f_l = 1$ and $N_{Tr} = 1$), $N_{AV} = 1024$ temporal trace averaging and with frequency sampling step $\delta = 1$ MHz, in a standard fiber with $\Delta\nu_B = 27$ MHz and 0.2 dB/km attenuation.

Table 1 illustrates the historical evolution of the figure-of-merit for BOTDA sensors achieved using different implementations, approximated for consistence and readability to two significant digits. It can be observed how this FoM has been significantly improved using innovative configurations during the past few years, mainly when aiming at reaching ultra-long sensing distances. Actually, extending the sensing range brings a big improvement in the figure-of-merit due to the exponential decay of the SNR with distance. This issue indicates that extending the sensing range of a Brillouin-based sensor is much more challenging than increasing the spatial resolution, which only impacts linearly on the SNR. In particular, systems with very high spatial resolution (typically short range, i.e. <5 km) are penalized by a small FoM mainly because Eq. (10) assumes that very high power (Watt levels) can be used, which is certainly not the case in the real implemented solutions currently reported in the literature. Possibly Eq. (10) should be modified for very high spatial resolution (<20 cm resolution, reaching typically a distance shorter than 5 km) to include specific limitations related to these configurations. This goes beyond the scope of the present study and will be addressed in a future work.

It is also important to mention that some of the references shown in Table 1 might result in an overestimated FoM; actually many of the results reported in the literature are clearly affected by pump depletion, a concern that has not always been properly addressed in many reported implementations.

Table 1. Historical Evolution of the Figure-of-merit for Distributed Optical Fiber Sensors Based on Brillouin Optical Time-domain Analysis

Date	Ref.	L [km] (sensing range)	Δz [m]	$N_{Tr} \cdot N_{AV}$ (per frequency)	δ [MHz]	$\Delta\nu_B$ [MHz]	σ_v [MHz]	FoM
Apr-93	[37] [a]	22	10	256	5	35	1.0	**2.0**
Sep-93	[38] [a]	32	5	512	5	35	1.0	**17.0**
Jul-95	[39] [a]	51	5	1024	5	35	1.0	**300.0**
Jun-98	[40] [a]	10	1	256	1	100	1.0	**1.0**
Sep-99	[41]	25	2	1000	12	70	10	**1.9**
Jul-08	[34]	5	0.3	16	1	300	1.0	**1.0**
		40	2	256	1	60	1.0	**6.8**
		50	7	256	1	30	1.0	**4.0**
Aug-09	[7]	12	1	1000	4	33	0.3	**0.7**
Jan-10	[19]	50	1	2048	5	60	2.2	**14.0**
May-10	[20]	50	0.5	4000	5	30	0.7	**45.0**
Aug-10	[14]	75	2	4000	2	65	4.0	**21.0**
Aug-10	[15]	100	2	16000	2	65	1.5	**290.0**
Sep-10	[42]	25	0.3	4000	5	30	1.0	**3.0**
		25	0.5	4000	5	30	0.5	**3.6**
Oct-10	[9]	5	0.05	512	1	27	1.5	**0.2**
Jan-11	[11]	100	2	4000	5	26	2.0	**440.0**
Jan-11	[24]	120	3	2000	3	50	3.1	**1'800.0**
Feb-11	[16]	120	2	5000	3	58.9	2.1	**2'800.0**
Mar-12	[8]	2	0.02	4000	5	75	2.0	**0.1**
Mar-12	[25]	60	0.25	30660	3	28	1.2	**39.0**
Apr-12	[17]	100	2	65536	2	34	1.5	**110.0**
Apr-12	[12]	75 [b]	1	4000	5	30	1.24	**4'600.0**
		150	2	4000	5	30	1.49	**65'000.0**
May-12	[18]	100	0.5	131072	2	30	3.8	**110.0**
Oct-12	[43]	122	4	508	3	86	1.0	**13'000.0**
Oct-12	[29]	120	1	8000	5	100	1.3	**12'000.0**
Dec-12	[44]	82	10	2048	2	35.7	6.0	**5.7**
Jan-13	[45]	72	5	2000	5	45	1.8	**26.0**
May-13	[26]	50 [b]	2	1000	1	60	1.0	**99.0**
Jul-13	[22]	100	2	2000	1	60	0.8	**1'100.0**
Sep-13	[28]	93	0.5	30480	3	35	1.7	**350.0**
Sep-13	[46]	142.2	5	1024	3	56	1.5	**26'000.0**
Oct-13	[47]	154.4	5	4080	3	60	1.4	**45'000.0**
Jan-14	[30]	100 [b]	3	2032	2	50	1.5	**48'000.0**
		120 [b]	5	2040	2	33	1.9	**300'000.0**

[a] Laser wavelength = 1.3 μm; hence, the fiber attenuation is assumed to be α = 0.35 dB/km; for all the rest α = 0.2 dB/km, corresponding to a laser operating at 1550 nm.
[b] Fiber loop configuration, i.e. the fiber length is twice longer than the sensing range; therefore, $f_l = 1$ in Eq. (10); for all the rest $f_l = 0$ (standard fiber configuration).

5. Conclusion

Based on a simple physical and statistical modeling, a novel expression to predict the uncertainty on the determination of the Brillouin frequency shift in BOTDA sensors has been established and validated by a rigorous experimental verification. Using this expression the actual accuracy on the determination of the Brillouin frequency shift can be confidently predicted from a single measurement of the SNR in the sensor response at the receiver. The present analysis highlights all the relevant parameters that have to be considered to evaluate the performance of distributed Brillouin optical fiber sensors. Based on this analysis and considering the limitations imposed by nonlinear effects and pump depletion, a solid figure-of-merit is introduced. This FoM should assist specialists in fairly evaluating the real progress

brought by proposed solutions presumably improving the performance of distributed Brillouin fiber sensors.

The authors wish that the presented analysis and proposed expressions will stimulate the community in the future to systematically inform about the full set of experimental parameters making the calculation of the FoM possible. This should generate a collegial emulation for achieving real progress and milestones in this promising field.

Appendix

In this appendix the error on the estimated peak Brillouin-gain frequency described in Eqs. (7) and (8) is derived in the case of a quadratic least-square fitting [31] of a measured Brillouin spectrum. This analysis is actually valid by extension for any system in which the central value of a resonance must be evaluated by fitting experimental points.

First, let consider that the measured local Brillouin gain spectrum (at a given position) is fitted by the following quadratic function:

$$y(x) = a \cdot x^2 + b \cdot x + c, \tag{11}$$

where the coefficients a, b and c are estimated from the least-square fitting. Then, using those coefficients, the estimated peak gain frequency v_B can be simply determined from:

$$\frac{dy}{dx} = 2a \cdot v_B + b = 0 \quad \Rightarrow \quad v_B = \frac{-b}{2a}. \tag{12}$$

Considering that the measured Brillouin traces are affected by additive Gaussian uncorrelated noise, the error on the estimation of v_B can be determined from the errors on the coefficients a and b as follows:

$$\sigma_v^2 = \left| \frac{\partial v_B}{\partial a} \right|^2 \sigma_a^2 + \left| \frac{\partial v_B}{\partial b} \right|^2 \sigma_b^2 + 2 \frac{\partial v_B}{\partial a} \frac{\partial v_B}{\partial b} \text{cov}_{a,b}, \tag{13}$$

where σ_a^2 and σ_b^2 are the variances of the coefficients a and b respectively, and $\text{cov}_{a,b}$ is the covariance between a and b.

While the variances of the coefficients a and b in this case are given by the diagonal elements of the covariance matrix that describes the system, the off-diagonal elements of this matrix describe the covariance between the different coefficients of the parabola [31]. Generally the off-diagonal elements are non-zero, and therefore, the factor $\text{cov}_{a,b}$ in Eq. (13) cannot be neglected. However, if the data points involved in the quadratic fitting are uniformly distributed (i.e. when the BGS is measured using a uniform frequency step) and they are symmetrically distributed around the peak value, the mathematical expressions for the factors σ_a and σ_b can be significantly simplified, while the factor $\text{cov}_{a,b}$ vanishes completely [31].

Thus, in order to simplify the mathematical expression for the error in Eq. (13), and without losing generality in the solution, the x-axis (i.e. frequency range used in the BGS measurements) can be shifted by a constant offset, so that the expected peak Brillouin-gain frequency v_B is positioned at the origin $x = 0$, leading in this way to a very small coefficient b (in fact, under this assumption $b = 0$ when v_B is exactly in the center of the frequency range used for the fitting). Thus, under such a condition, and following the mathematical description presented in [31], based on the statistical error analysis of the least-square-fitting method, the factors σ_a, and σ_b can be easily extracted:

$$\sigma_a^2 = \frac{5\sigma^2}{4N\sigma_x^4}, \tag{14}$$

$$\sigma_b^2 = \frac{\sigma^2}{N\sigma_x^2}, \tag{15}$$

where N is the number of data points used in the fitting, σ^2 is the variance of the Gaussian noise affecting the measured traces, and σ_x^2 is the variance of the uniformly distributed data points, which can be algebraically calculated as:

$$\sigma_x^2 = \frac{\left(N^2 - 1\right) \cdot \delta^2}{12},$$ (16)

where δ is the spacing of the data points, which represents in this case the frequency step between the successive acquisition of Brillouin traces.

Using Eq. (16) and considering that the number of frequency points N involved in the fitting is large enough, so that $N^2 \gg 1$, the error on the estimation of the coefficients a and b can be obtained:

$$\sigma_a^2 = \frac{180\sigma^2}{N^5 \delta^4},$$ (17)

$$\sigma_b^2 = \frac{12\sigma^2}{N^3 \delta^2}.$$ (18)

It must be pointed out that the condition of a large number of fitted points is already satisfied with a good approximation when N is larger than 3. In all cases a smaller number of sampling points is simply mathematically irrelevant to determine a parabolic function, since it is generically characterized by 3 parameters, as expressed in Eq. (11).

Replacing Eqs. (17) and (18) into Eq. (13), the following expression for the error on the estimated local Brillouin frequency shift can be obtained:

$$\begin{aligned}
\sigma_\nu^2 &= \frac{b^2}{4a^4}\sigma_a^2 + \frac{1}{4a^2}\sigma_b^2 = \frac{b^2}{4a^4}\frac{180\sigma^2}{N^5\delta^4} + \frac{1}{4a^2}\frac{12\sigma^2}{N^3\delta^2} \\
&= \frac{\sigma^2}{a^2 N^3 \delta^2}\left[\frac{b^2}{4a^2}\frac{180}{N^2\delta^2} + 3\right] \\
&= \frac{\sigma^2}{a^2 N^3 \delta^2}\left[\frac{180 \cdot \nu_B^2}{N^2\delta^2} + 3\right].
\end{aligned}$$ (19)

Note that the expression in Eq. (19) depends on the coefficient a, which actually defines the curvature of the fitted parabola, and hence, it is expected to have a direct relation with the Brillouin FWHM linewidth. In order to obtain a relation independent of the fiber location (i.e. to neglect the effects of the fiber attenuation on the coefficients of the parabola), the local Brillouin gain can be normalized, as shown in Fig. 5, so that the maximum peak response is equal to 1 at the resonance frequency, while in absence of gain the response is 0. Under such an assumption, the following relation between the coefficients of the fitted parabola must be satisfied at the resonance Brillouin frequency:

$$y\left(x = \frac{-b}{2a}\right) = a \cdot \left(\frac{-b}{2a}\right)^2 + b \cdot \left(\frac{-b}{2a}\right) + c = 1$$

$$\Rightarrow \frac{-b^2}{4a} + c = 1.$$ (20)

Using Eq. (20) and assuming that the fitting is carried out considering only data points above a given threshold level η (with $0 < \eta < 1$) defined by the range $\nu_B - x_\eta \le x \le \nu_B + x_\eta$, where $y(x = \nu_B \pm x_\eta) = \eta$, the following expression for the coefficient a can be extracted:

$$y\left(\nu_B \pm x_\eta\right) = a \cdot \left(\nu_B \pm x_\eta\right)^2 + b \cdot \left(\nu_B \pm x_\eta\right) + c = \eta$$

$$\Rightarrow a = \frac{\eta - 1}{x_\eta^2}.$$ (21)

Considering that $N \gg 1$, and that the frequency range which is used for the fitting is $2x_\eta$, where $2x_\eta = (N-1) \cdot \delta \approx N \cdot \delta$, the expression for the coefficient a can be written as:

$$a = \frac{4(\eta - 1)}{N^2 \delta^2}. \tag{22}$$

It is important to point out that Eq. (22) is valid for every level η with $0 < \eta < 1$. Consequently, by evaluating the parabola at the Brillouin FWHM it is possible to obtain the following relation between the number of data points N involved in the fitting, the frequency spacing δ, the discrimination level η, and the Brillouin FWHM linewidth Δv_B:

$$a = \frac{4(\eta - 1)}{N^2 \delta^2} = \frac{-2}{\Delta v_B^2}$$
$$\Rightarrow N^2 \delta^2 = 2 \cdot \Delta v_B^2 \cdot (1 - \eta). \tag{23}$$

Then, replacing Eqs. (22) and (23) into Eq. (19), the error on the estimated Brillouin frequency shift can be obtained as:

$$\sigma_v^2 = \frac{\sigma^2 \delta \cdot \Delta v_B}{8\sqrt{2} (1-\eta)^{3/2}} \left[\frac{180}{2(1-\eta)} \frac{v_B^2}{\Delta v_B^2} + 3 \right]. \tag{24}$$

Note that the first factor inside the brackets in Eq. (24) can be neglected in many practical cases since the factor $(v_B / \Delta v_B)^2$ is normally very small (in fact v_B is nearly equal to zero as a result of the centering frequency offset). Actually, this factor depends on how symmetric the data points are distributed around the peak-gain frequency; and therefore, the impact of the first term in the brackets of Eq. (24) can be made negligible if the frequency data points are symmetrically distributed around v_B. On the contrary, if the range of frequencies used for the fitting ($v_B - x_\eta \leq x \leq v_B + x_\eta$) is not well-centered with respect to v_B, the error in the estimated Brillouin frequency shift is expected to increase rapidly. In order to reduce the frequency error resulting from data points asymmetrically located with respect to the peak v_B, an iterative multi-pass fitting procedure can be carried out to adjust recursively the frequency range and keep it symmetrically centered with respect to the peak-gain frequency v_B.

In addition, it is worth pointing out that the error introduced by the first factor in Eq. (24) can also significantly increase if the threshold level η used in the fitting approaches 1, independently of the number of frequency data points employed. Therefore, the threshold level η for the fitting has to be kept below a reasonable value (for instance below 0.7, as illustrated in Fig. 11), so that the variance of the error in the Brillouin frequency estimation (in a well-centered spectrum) can be reduced to:

$$\sigma_v^2 = \frac{3\sigma^2 \delta \cdot \Delta v_B}{8\sqrt{2} (1-\eta)^{3/2}}. \tag{25}$$

Note that, due to the normalization of the Brillouin gain spectrum, the factor σ in Eq. (25) corresponds to the inverse of the SNR of the trace at the maximum gain, so that the frequency error resulting from the quadratic fitting procedure can be expressed as:

$$\sigma_v = \sqrt{\frac{3}{8\sqrt{2} (1-\eta)^{3/2}}} \frac{\sqrt{\delta \cdot \Delta v_B}}{SNR}. \tag{26}$$

For instance, in the particular case of $\eta = 0.5$ (i.e. when the fitting of the BGS considers the data points within the Brillouin FWHM linewidth only), the frequency error can be estimated by the following expression:

$$\sigma_v = \frac{1}{SNR} \sqrt{\frac{3}{4} \cdot \delta \cdot \Delta v_B}. \tag{27}$$

Equation (27) provides an estimation of the local frequency error (and hence, the respective temperature and strain resolution) resulting from the least-square quadratic fitting

on the local BGS, as a function of the measurement frequency step, the Brillouin linewidth and the local SNR.

The functional dependence of the local frequency error on the different measurement parameters is actually logical and supports the assumption that it does not depend on the type of fitting that is performed over the measured points. This can be better figured out by re-expressing Eq. (27) under the following form:

$$\sigma_\nu = \frac{1}{SNR}\sqrt{\frac{3}{4}\frac{\delta}{\Delta\nu_B}}\Delta\nu_B = \sigma\sqrt{\frac{3}{4}}\frac{\Delta\nu_B}{\sqrt{N}}. \tag{28}$$

Equation (28) shows that the local frequency error σ_ν is logically proportional to the noise on the sensor response σ and to the width of the resonance $\Delta\nu_B$, and is inversely proportional to the square root of the number of sampling points N. This latter dependence is usual in statistical estimations of the standard deviation of a quantity, so that the functional dependence is not expected to essentially change if a more sophisticated fitting is carried out. Only the numerical factor $\sqrt{3/4}$ can be reasonably taken as specific to the type of function fitted over the experimental points and could be potentially made smaller.

Acknowledgments